Available online at www.sciencedirect.com
SCIENCE DIRECT®
Journal of Nuclear Materials 335 (2004) 345–352
journal of nuclear materials
www.elsevier.com/locate/jnucmat

Thermodynamic modelling of $LiF–LnF_3$ and $LiF–AnF_3$ phase diagrams

J.P.M. van der Meer [a,*], R.J.M. Konings [a], M.H.G. Jacobs [b], H.A.J. Oonk [b]

[a] European Commission, Joint Research Centre, Institute for Transuranium Elements, P.O. Box 2340, 76125 Karlsruhe, Germany
[b] Petrology Group, Utrecht University, Budapestlaan 4, 3584 CD Utrecht, The Netherlands

Received 4 March 2004; accepted 5 July 2004

Abstract

The phase diagrams of the $LiF–LnF_3$ series, where Ln = La–Sm, and of $LiF–AnF_3$, where An = U, Pu, have been optimized using Redlich–Kister functions. The phase diagrams of $LiF–AmF_3$ and $LiF–PuF_3–AmF_3$ have been calculated. The necessary Gibbs energy functions for americium trifluoride were defined by use of a semi-empirical method. The excess Gibbs energy terms, which are expressed as Redlich–Kister polynomials and describe the effect of interaction between the two fluoride components in the liquid phase, were obtained by translating the trends observed in the lanthanide trifluoride series into the actinide series. A single eutectic has been found in the $LiF–AmF_3$ system with the eutectic point at $\simeq$33 mole% AmF_3 and at $\simeq$951 K.

1. Introduction

The research on a nuclear reactor using molten salt fuel started in the USA in the early 1950s with the design of a nuclear-powered aircraft, using a circulating molten fluoride salt. Later, the emphasis shifted to the development of a civilian power reactor based on the same principle. An intensive research programme was performed on molten fluoride salt systems in the Molten Salt Reactor Experiment at the Oak Ridge National Laboratory during the 1960s. The molten salt fuels were based in general on UF_4 and/or ThF_4 kept in solution in a mixture of ZrF_4, NaF, LiF and BeF_2 in different amounts. Their stability at high temperatures and resistance against radiation made the fluoride salts attractive for this purpose [1].

The Molten Salt Reactor was originally designed as a breeder using uranium or plutonium to start up the reactor to produce U-233 from Th-232. In a later stage, the possibility to use the reactor as a burner of plutonium and other actinides became an option as well. In the USA, the support for the Molten Salt Reactor ceased in 1975. However, the fluoride salts have become subject to renewed interest since 1990s in the frame of the Partitioning and Transmutation (P&T) and Generation IV programmes.

In this context it is of great importance to understand the behavior of the minor actinide fluoride components. Thermal analysis of these, in general, highly active substances, is complicated and for most actinide compounds, it has not been carried out yet. In contrast, more information is available for lanthanide compounds.

* Corresponding author.
E-mail address: juliette.vandermeer@itu.fzk.de (J.P.M. van der Meer).

0022-3115/$ - see front matter © 2004 Elsevier B.V. All rights reserved.
doi:10.1016/j.jnucmat.2004.07.035

Thermal analysis [2–8] as well as calorimetry [9,10] have been carried out on lanthanide fluoride systems.

In this work, the phase diagram of the system lithium fluoride–americium trifluoride was calculated by means of estimated excess Gibbs energy coefficients, expressed as Redlich–Kister polynomials and recently assessed Gibbs energy functions. Estimations for the excess terms of AmF_3 were achieved by observing the trends in the lanthanide series and inferring probable excess terms. The Gibbs energy functions for AmF_3 were obtained by a semi-empirical method.

2. Method

2.1. Gibbs energy functions

Gibbs energy functions have been set up by careful investigation of existing thermodynamic tables in such a way that it could be described as the polynomial in Eq. (1):

$$G(T) = a + bT + cT\ln(T) + \sum d_i T^i. \tag{1}$$

Gibbs energy functions have been defined for each phase. The enthalpy as well as the entropy can be obtained from the heat capacity values (Eqs. (2)–(4)). H_{ref} is the enthalpy at the reference state, which is the enthalpy of formation at 298.15 K.

$$G(T) = H(T) - S(T)T, \tag{2}$$

$$H(T) = H_{\mathrm{ref}} + \int_{T_{\mathrm{ref}}}^{T} C_p \,\mathrm{d}T, \tag{3}$$

$$S(T) = \int_{T=0}^{T} \frac{C_p}{T}\,\mathrm{d}T. \tag{4}$$

Thermal and calorimetric data are abundant for many fluoride compounds, such as LiF, e.g. [11–14]. Also for the lanthanide trifluorides [9,10,15] and for some actinide trifluorides [16–18], reliable thermodynamic data and good estimated data are available. On the contrary, for several compounds, such as AmF_3, the heat capacity has not been measured yet. To achieve a good estimation of the C_p function, a semi-empirical method has been applied.

It is assumed that the standard entropy S^0 for lanthanide and actinide compounds can be described as the sum of a lattice component and an excess component [18,19]. The former arises from the lattice vibrations and can be considered as a base contribution through the complete range of the lanthanides or the actinides with the same crystal structure; the latter depends on the electronic configuration of the lanthanide or actinide considered and can be calculated from the crystal field energy. As the entropy is related to the heat capacity, the same method has been used for calculating the C_p of AmF_3. The heat capacity data of UF_3, which are well known [16], were taken initially. Subtracted were the electronic excess values for the U^{3+} ion, which have been calculated from the crystal field energies of U^{3+} in UCl_3. It was assumed that the crystal field contribution for trichlorides is similar to that for trifluorides, resulting in a lattice heat capacity component for actinide trifluoride. Subsequently, the calculated electronic component for AmF_3 was added.

2.2. Redlich–Kister coefficients

The excess Gibbs energy parameters, which are necessary to define the T–X phase diagram, are unknown for the majority of the systems concerned. To calculate the phase diagrams, the excess parameters are optimized by fitting the Gibbs energy function to known experimental data. Redlich–Kister polynomials are used to describe the excess parameters and are defined as in Eq. (5) for binary systems.

$$\Delta_{xs}G = X_{\mathrm{A}}X_{\mathrm{B}}\sum_{k=0}^{N} {}^{k}L_{\mathrm{A,B}}(X_{\mathrm{A}} - X_{\mathrm{B}})^k. \tag{5}$$

${}^{k}L_{\mathrm{A,B}}$ are the interaction coefficients, which are defined as a linear function of the temperature.

$${}^{k}L_{\mathrm{A,B}} = {}^{k}p_{\mathrm{A,B}} + {}^{k}q_{\mathrm{A,B}}T. \tag{6}$$

The coefficients ${}^{k}p_{\mathrm{A,B}}$ and ${}^{k}q_{\mathrm{A,B}}$, where A is LiF and B is XF_3, are optimized by use of the ChemSage [20] optimization module. It uses the Bayesian Optimization Algorithm, a genetic algorithm, which is based on a probability model [21], to obtain an optimum fit between the theoretical Gibbs energy functions and the experimental values. Optimizations have been carried out for LiF–LnF_3 (Ln = La, Ce, Pr, Nd, Sm) and for LiF–AnF_3 (An = U, Pu) binary systems. The resulting excess Gibbs energy coefficients were used to estimate the coefficients for LiF–AmF_3.

2.3. The LiF–PuF_3–AmF_3 ternary diagram

The ternary LiF–PuF_3–AmF_3 diagram was calculated under a few assumptions: The first was that no ternary interactions exist between the components. Second, it was assumed that AmF_3 and PuF_3 form an ideal solid solution. This was based on the fact that both compounds are isostructural with a hexagonal structure and that the difference between the effective ionic radii

of Am^{3+} and Pu^{3+} is small (97.5 and 100.0 pm, respectively [22]).

3. Results

3.1. The $LiF–LnF_3$ and $LiF–AnF_3$ diagrams

The phase diagrams of the $LiF–LnF_3$ series, where Ln = (Ln–Sm) all show a single eutectic without the formation of an intermediate compound [6]. Details can be found in Table 1, which lists the calculated and the experimentally determined eutectic points. Enthalpies of mixing are not known, except for the system $LiF–LaF_3$, of which the enthalpies have been measured by Hong and Kleppa [9] and Abdoun et al. [10]. This is therefore the only system in this study for which the mixing enthalpies have been included in the optimization, although the difference in the result between in- or excluding is negligible.

Similar calculations have been performed for the series of $LiF–AnF_3$, with An = (U, Pu). The system $LiF–PuF_3$ has been thoroughly measured by Barton and Strehlow [23], but data on $LiF–UF_3$, which are based on an unpublished report by Barton et al. given in [7], are scattered and less precise. The resulting diagram, although a single eutectic binary system as well, has a distinctly different shape when compared to the others. Since such a deviating shape was not expected, the diagram was recalculated using interpolated excess coefficients. The way it was done is discussed below. A remark should be made on the Gibbs energy functions used for liquid UF_3 and PuF_3. The entropy of fusion $\Delta_{fus} S$, one of the parameters to describe $G^{liq}(T)$, was for both compounds taken as 33 $JK^{-1}mol^{-1}$, instead of 20.8 $JK^{-1}mol^{-1}$, proposed by Rand and Fuger [17]. The former value seemed to be more consistent with the entropies of fusion for the analogous lanthanide fluorides, which are well known.

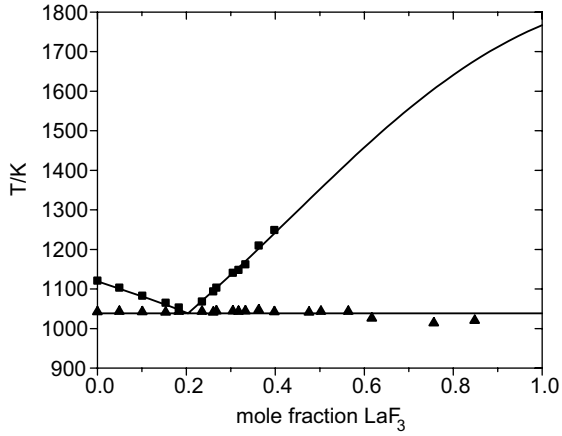

Fig. 1. The optimized $LiF–LaF_3$ phase diagram: (■) experimental data liquidus; (▲) experimental data solidus, both by Thoma et al. [6].

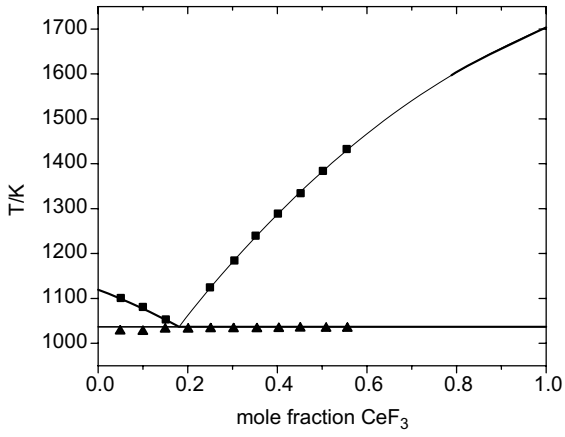

Fig. 2. The optimized $LiF–CeF_3$ phase diagram: (■) experimental data liquidus; (▲) experimental data solidus, both by Barton et al. [2].

Table 1
Calculated and experimental eutectic points in the systems $LiF–XF_3$

X	x_e, mole% $XF_{3,calc}$	$T_e/K_{,calc}$	x_e, mole% $XF_{3,exp}$[a]	$T_e/K_{,exp}$[a]
La	21.2	1038.5	20.0	1043
Ce	18.5	1036.9	19.0[b]	1028
Pr	21.0	1030.6	19.0	1023
Nd	25.3	1006.5	23.0	1011
Sm	27.3	969.0	27.0[b]	971
U	28.1	1050.7	27.0[c]	1043
Pu	20.4	1009.0	19.5[d]	1016

[a] [6].
[b] [2].
[c] [28].
[d] [23].

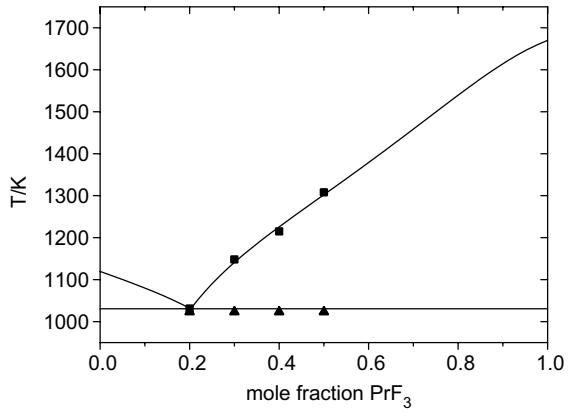

Fig. 3. The optimized LiF–PrF_3 phase diagram: (■) experimental data liquidus; (▲) experimental data solidus, both by Thoma et al. [6].

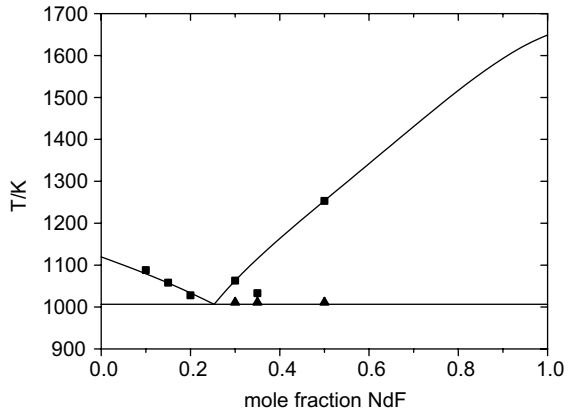

Fig. 4. The optimized LiF–NdF_3 phase diagram: (■) experimental data liquidus; (▲) experimental data solidus, both by Thoma et al. [6].

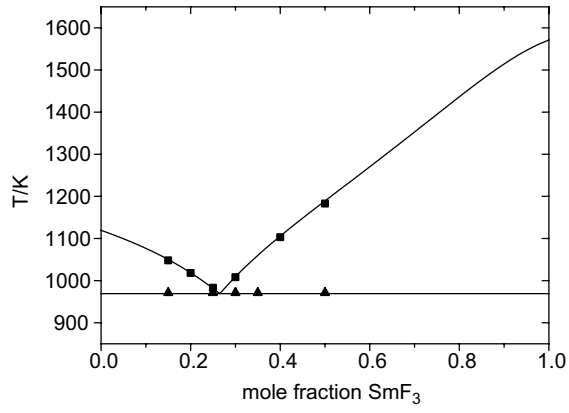

Fig. 5. The optimized LiF–SmF_3 phase diagram: (■) experimental data liquidus; (▲) experimental data solidus, both by Thoma et al. [6].

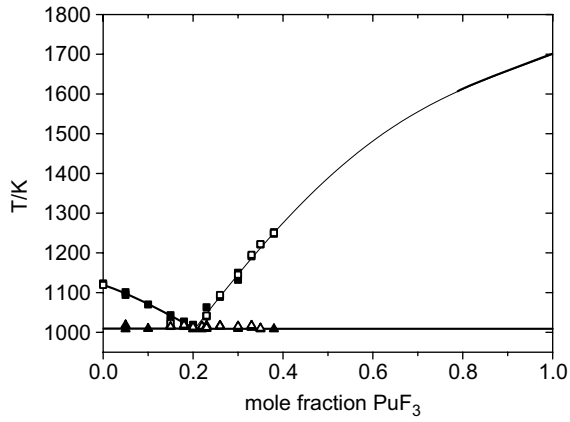

Fig. 6. The optimized LiF–PuF_3 phase diagram: (■) experimental data liquidus (thermal analysis); (▲) experimental data solidus (thermal analysis); (□) experimental data liquidus (potentiometer); (△) experimental data solidus (potentiometer), all by Barton and Strehlow [23].

Phase diagrams of the systems with other actinide fluorides have not been measured yet. The calculated diagrams are presented in Figs. 1–6.

3.2. The excess Gibbs energy coefficients

From our experience, it appeared that different pairs of excess coefficients can result in similar diagrams, so that the values obtained by ChemSage cannot be taken unambiguously. However, the data shown here are considered as those resulting in the best fits with the experimental data. The values are given in Table 2.

Values of ${}^{k}p_{A,B}$ and ${}^{k}q_{A,B}$ were plotted against the effective ionic radius of the cation X in XF_3. The result is shown in Fig. 7. Two clear non-linear trends are visible. Based on these trends, linear interpolations of the excess coefficients for the systems LiF–UF_3 and LiF–AmF_3 were made, using the effective ionic radii of U and Am and the values of the first neighboring ionic radii.

The interpolated values of the excess coefficients for LiF–UF_3 have been used to calculate the phase diagram. It has been shown in Fig. 8 that the result is in better agreement with the phase diagrams of the other LiF–XF_3 systems.

3.3. The diagrams of LiF–AmF_3 and LiF–PuF_3–AmF_3

The Gibbs energy function of the pure compound of AmF_3 was calculated by means of an estimated C_p func-

Table 2
Optimized and interpolated ${}^{k}p_{A,B}$ and ${}^{k}q_{A,B}$ for A is LiF and B is XF_3

X	${}^{0}p_{A,B}$ ($J\,mol^{-1}$)	${}^{0}q_{A,B}$ ($J\,K^{-1}\,mol^{-1}$)	${}^{1}p_{A,B}$ ($J\,mol^{-1}$)	${}^{1}q_{A,B}$ ($J\,K^{-1}\,mol^{-1}$)
La	−17848	−2.5323	−20810	10.880
Ce	−15265	2.0892	−7613.1	5.3094
Pr	3699.6	−13.545	16125	−15.979
Nd	13573	−18.931	15006	−15.504
Sm	5291.9	−22.673	12359	−13.621
U	6088.0	−21.584	9822.0	−25.650
U_{int}[a]	−17026	−1.0618	−16611	9.1073
Pu	10015	−17.315	−3804.5	8.4936
Am	10923	−20.129	13415	−13.948

[a] U_{int} for interpolated values.

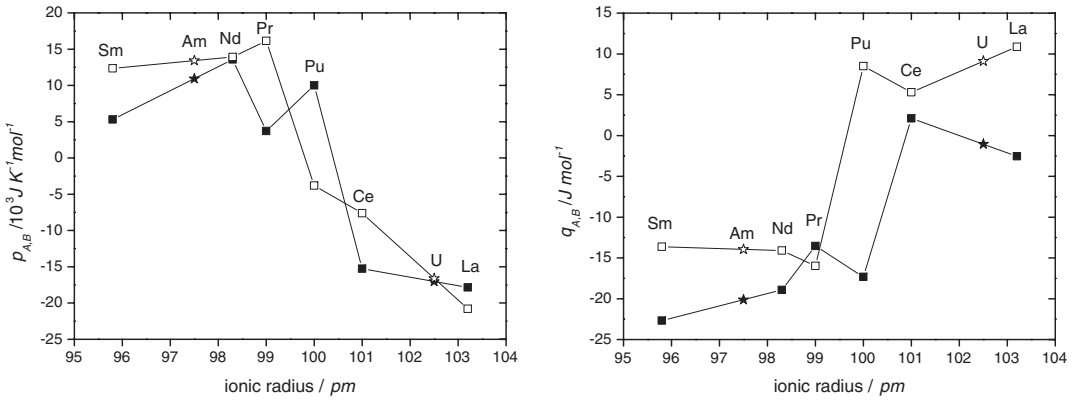

Fig. 7. The optimized Redlich–Kister coefficients ${}^{k}p_{A,B}$ and ${}^{k}q_{A,B}$ of systems LiF–XF_3 versus the effective ionic radius of cation X, according to Shannon [22]. Solid symbols represent values for $k = 0$, open symbols for $k = 1$. Star symbols are interpolated values.

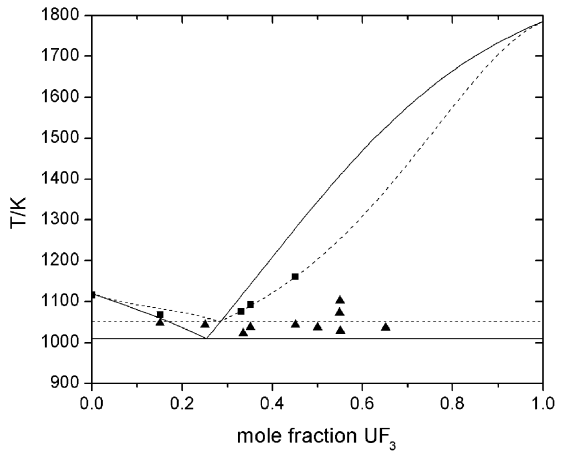

Fig. 8. The optimized LiF–UF_3 phase diagram: (– – –) optimized in ChemSage; (—) based on interpolated excess Gibbs values for UF_3-LiF; (■) unpublished experimental data liquidus; (▲) unpublished experimental data solidus, both by Barton et al. [28]. Data points below 900 K have been omitted.

tion, which can be found in Appendix A. The resulting G functions of the pure solid as well the liquid state are described by Eqs. (7) and (8):

$$G^{sol}_{AmF_3}(T) = -1.619\times10^{6} + 5.154\times10^{2}\,T - 9.148\times10^{1}\,T\ln(T) - 1.509\times10^{-2}\,T^{2} + 1.356\times10^{-6}\,T^{3} + 4.142\times10^{5}\,T^{-1}, \quad (7)$$

$$G^{liq}_{AmF_3}(T) = -1.619\times10^{6} + 7.797\times10^{2}\,T - 1.300\times10^{2}\,T\ln(T). \quad (8)$$

As was explained in the previous section, values for the excess parameters, ${}^{k}p_{A,B}$ and ${}^{k}q_{A,B}$, were achieved by interpolation based on the trends found in Fig. 9. The resulting diagram is shown in Fig. 7. A binary eutectic point has been found at 32.7 mole% AmF_3 at 951 K.

The calculated ternary LiF–PuF_3–AmF_3 phase diagrams is shown in Fig. 10. With intervals, it shows the liquid stability fields above 1009 K, which is the binary eutectic temperature of LiF–PuF_3.

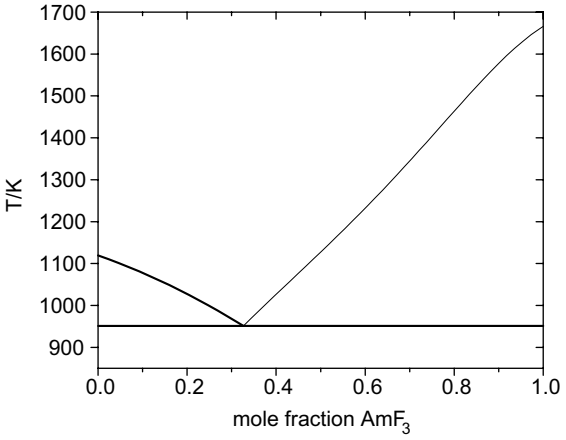

Fig. 9. The calculated $LiF–AmF_3$ phase diagram.

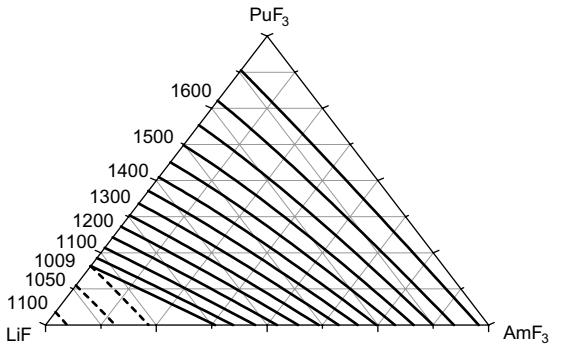

Fig. 10. The calculated $LiF–PuF_3–AmF_3$ ternary phase diagram from 1009 to 1650 K with a temperature interval of 50 K starting at 1050 K. (– – –) LiF (sol) stable; (—) $(Pu,Am)F_3$ (ss) stable.

4. Discussion

4.1. $LiF–LnF_3$ systems

The phase diagrams in this paper have all been optimized according to the Redlich–Kister polynomial model using the Bayesian Optimization Algorithm. Evidently, the fit improves when more accurate data are available. The problem is that, except for $LiF–LaF_3$, no enthalpies of mixing are known, so that too many degrees of freedom are present to fix the solutions properly. Therefore, the optimized Redlich–Kister coefficients for the same system could differ. Moreover, the coefficients were dependent on the starting values for the Bayesian algorithm, although the resulting phase diagrams appeared to be similar. The Bayesian Optimization Algorithm optimizes the total excess Gibbs energy, which is described by an excess enthalpy and an excess entropy term. In order to reduce the number of variables, the optimization was performed with less parameters, for example only one ${}^{k}p_{A,B}$ and one ${}^{k}q_{A,B}$ coefficient, but it appeared that the description of the diagrams was not acceptable.

4.2. $LiF–AnF_3$ systems and the modelling of $LiF–AmF_3$

It was assumed in the modelling of $LiF–AmF_3$, that the binary systems with lanthanide and actinide fluorides behave in a similar way. Since the phase diagrams are analogous, this is probably correct. It is also supported by the evidence that the ionic radii of the actinides follow a trend corresponding to that of the lanthanides. It is known that in the heavier $LiF–LnF_3$ series, from EuF_3 on, intermediate compounds $LiF \cdot LnF_3$ are being formed. It might be questioned whether this is also the case for $LiF–AmF_3$. However, it is noted that in the lanthanide series, the formation of compounds coincides with the change from a trigonal/hexagonal to an orthorhombic structure. Since AmF_3 has the same crystal structure as LaF_3 [24], it is probable that the compound $LiF \cdot AmF_3$ is not stable.

4.3. Models

The model used to calculated the phase diagrams was the Redlich–Kister model. This is a pure mathematical model and it is difficult, if not impossible, to attribute a physical sense to it. Its major advantage is that fair descriptions can be achieved with the minimum of unknown parameters. Alternatively, other models with a physical meaning, such as an ionic liquid or a sublattice model can be used; however, the drawback is that hardly any physical parameters are known of the fluoride compounds. Good estimates have to be found then for a proper application. These physical models will be studied in the future as well, to compare the results and to improve the validity of the estimation and calculation of phase diagrams.

4.4. $LiF–PuF_3–AmF_3$ ternary diagram

Typical salt compositions for a waste burner contain about four times more PuF_3 than AmF_3. Fig. 11 shows the pseudobinary system $LiF–Pu_{0.8}Am_{0.2}F_3$. The x-axis would be the connecting line from the LiF apex to the $AmF_3–PuF_3$ side at a mole fraction of 0.20 AmF_3 in the ternary diagram.

Studying the pseudobinary diagram, it can be seen that the temperature where the first melt appears is 1001 K, at a mole fraction of 0.78 LiF. This temperature is significantly higher than for the standard MSR fuel compositions. The liquidus temperature for typical compositions based on a $LiF–BeF_2$ solvent is $\simeq$870 and $\simeq$775 K for a fuel based on $NaF–ZrF_4$. The characteristic inlet temperature of the primary salt in the Oak Ridge MSBR

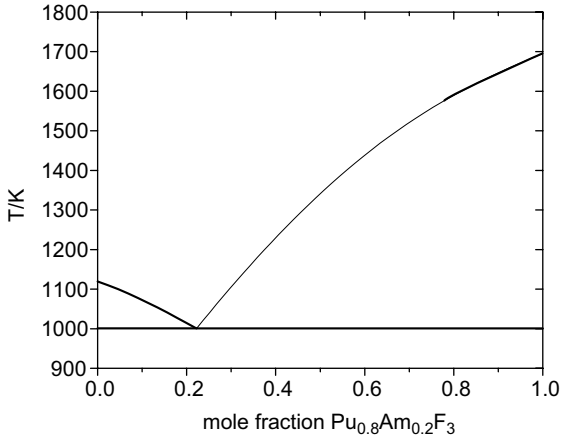

Fig. 11. The pseudobinary LiF–$Pu_{0.8}Am_{0.2}F_3$ phase diagram.

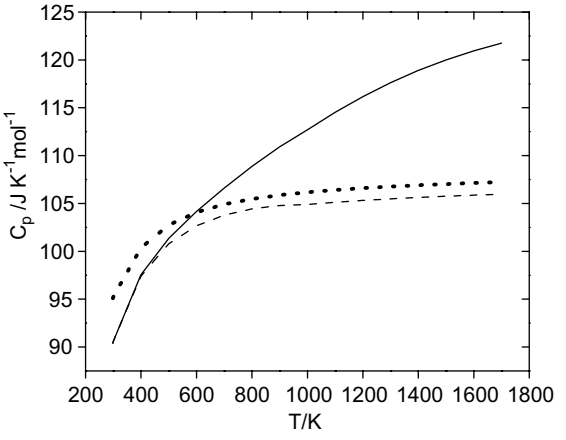

Fig. 12. Heat capacity versus temperature: (···) C_p of UF_3; (–––) C_{lat} of UF_3; (—) C_p of AmF_3.

(breeder) design was 839 K, whilst the outlet temperature was 978 K. Apparently, pure LiF is not suitable as a solvent and the addition of a second component, such as BeF_2 would be necessary, despite its toxicity. For that reason, analysis of the system LiF–BeF_2–AnF_3 will be performed in the future.

5. Conclusion

The original concept for a Molten Salt Reactor was based on the use of a molten LiF–BeF_2 salt as a carrier. Since BeF_2 is very toxic, research is being performed for a reactor concept with solely LiF as the matrix salt. This study has only dealt with the melting temperatures of several compositions with LiF and indicates that the melting temperature is greater than 1000 K, probably too high for a future reactor.

Acknowledgment

The authors thank Dr Klaus Hack from GTT Technologies, Aachen for support in working with the ChemSage software.

Appendix A. Estimation of the C_p of AmF_3

The heat capacity function of pure AmF_3 in the solid state was estimated as follows. The heat capacity function of UF_3 measured by Cordfunke et al. [25] has been taken. The excess contribution, generated by the electronic configuration, is not known for UF_3, but it could be calculated for UCl_3, under the assumption that the electronic contributions of the U^{3+} ions are similar. The calculations are explained in Eqs. (A.1) and (A.2) [26]:

$$C_p^0 = C_{\text{lat}} + C_{\text{elec}}, \tag{A.1}$$

$$C_{\text{elec}} = Q^{-2} R^{-1} T^{-2} \left[Q \sum_{i=1}^{n} g_i E_i^2 \exp(-E_i/RT) - \left(\sum_{i=1}^{n} g_i E_i \exp(-E_i/RT) \right)^2 \right], \tag{A.2}$$

$$Q = \sum_{i=0}^{n} g_i \exp(-E_i/RT). \tag{A.3}$$

Q is the partitioning function described by the Maxwell–Boltzmann distribution law (Eq. (A.3)), T is the absolute temperature, R the universal gas constant, E_i the energy of level i and g_i its degeneracy.

The lattice heat capacity was obtained from the total heat capacity function for UF_3, subtracting the electronic contribution for the U^{3+} ion. Subsequently, the electronic contribution of the Am^{3+} ion was calculated, with the same assumptions, and added to the lattice function. In absence of data on the electronic energy levels, the crystal field energies, for the actinide trifluorides, the C_{elec} terms have been calculated for the data for the corresponding chloride systems [27]. Fig. 12 shows the relations of C_{lat} and C_{elec} of UF_3 and AmF_3.

References

[1] H.G. MacPherson, Nucl. Sci. Eng. 90 (1985) 374.
[2] C.J. Barton, L.M. Bratcher, R.J. Sheil, W.R. Grimes, Oak Ridge National Laboratory, unpublished.

[3] G.A. Bukhalova, E.P. Babaeva, Russ. J. Inorg. Chem. 10 (1965) 1026.
[4] G.A. Bukhalova, E.P. Babaeva, T.M. Khliyan, Russ. J. Inorg. Chem. 10 (1965) 1158.
[5] R.E. Thoma, H. Insley, G.M. Hebert, Inorg. Chem. 5 (1966) 1222.
[6] R.E. Thoma, G.D. Brunton, R.A. Penneman, T.K. Keenan, Inorg. Chem. 9 (1970) 1096.
[7] R.E. Thoma, Advances in Molten Salt Chemistry, vol. 3, Plenum, 1975, p. 275 (Chapter 6).
[8] A.I. Agulyanskii, V. Bessonova, Russ. J. Inorg. Chem. 27 (1982) 579.
[9] K.C. Hong, O.J. Kleppa, J. Phys. Chem. 83 (1979) 2589.
[10] F. Abdoun, M. Gaune-Escard, G. Hatem, J. Phase Equil. 18 (1997) 6.
[11] M.W. Chase Jr., NIST-JANAF Thermochemical Tables, 4th Ed., Part I, Al–Co, J. Phys. Chem. Ref. Data Monograph 9.
[12] K. Clusius, W. Eishenauer, Z. Naturforsch. A 2 (1956) 715.
[13] T.B. Douglas, J.L. Dever, J. Amer. Chem. Soc. 76 (1954) 4826.
[14] N.K. Voskresenskaya, V.A. Sokolov, E.I. Banashek, N.E. Shmidt, Akad. Nauk SSSR, Izvest. Sect. Fiz. Khim. Anal. 27 (1956) 233.
[15] R.J.M. Konings, A. KovácsHandbook on the Physics and Chemistry of Rare Earths, vol. 33, North-Holland, Amsterdam, 2003, p. 147 (Chapter 213).
[16] I. Grenthe, J. Fuger, R.J.M. Konings, R.E. Lemire, A.B. Muller, C. Nguyen-Trung, H. Wanner, Chemical Thermodynamics of Uranium, North-Holland, Amsterdam, 1992.
[17] M.H. Rand, J. Fuger, Technical report, EUR 17322 EN, 2000.
[18] R.J.M. Konings, J. Chem. Thermodyn. 36 (2004) 121.
[19] R.J.M. Konings, J. Nucl. Mater. 295 (2001) 57.
[20] G. Eriksson, K. Hack, Metall. Trans. B 21 (1990) 1013.
[21] M. Pelikan, D.E. Goldberg, E. Cantú-Paz, in: Proceedings of the Genetic and Evolutionary Computation Conference, 1999, p. 525.
[22] R.D. Shannon, Acta Crystallogr. A 32 (1976) 751.
[23] C.J. Barton, R.A. Strehlow, J. Inorg. Nucl. Chem. 18 (1961) 143.
[24] R.J. Silva, G. Bidoglio, M.H. Rand, P.B. Robouch, H. Wanner, I. Puigdomenech, Chemical Thermodynamics of Americium, North-Holland, Amsterdam, 1995.
[25] E.H.P. Cordfunke, R.J.M. Konings, E.F. Westrum Jr., J. Nucl. Mater. 167 (1989) 205.
[26] S. Lutique, P. Javorský, R.J.M. Konings, A.C.G. van Genderen, J.C. van Miltenburg, F. Wastin, J. Chem. Thermodyn. 35 (2003) 955.
[27] W.T. Carnall, J. Chem. Phys. 95 (1991) 7195.
[28] C.J. Barton, V.S. Coleman, L.M. Bratcher, R.R. Grimes, Oak Ridge National Laboratory, unpublished.